Conference Applications of Mathematics 2013
in honor of the 70th birthday of Karel Segeth.
Jan Brandts, Sergey Korotov, Michal Křížek,
Jakub Šístek, and Tomáš Vejchodský (Eds.),
Institute of Mathematics AS CR, Prague 2013

ON MATHEMATICAL MODELLING OF GUST RESPONSE USING THE FINITE ELEMENT METHOD

Petr Sváček[1], Jaromír Horáček[2]

[1] Czech Technical University in Prague, Faculty of Mechanical Engineering
Department of Technical Mathematics
Karlovo nám. 13, 121 35 Praha 2, Czech Republic
e-mail: Petr.Svacek@fs.cvut.cz
[2] Institute of Thermomechanics, Academy of Sciences of the Czech Republic
Dolejškova 5, 182 00 Praha 8, Czech Republic
email: jaromirh@it.cas.cz

Abstract

In this paper the numerical approximation of aeroelastic response to sudden gust is presented. The fully coupled formulation of two dimensional incompressible viscous fluid flow over a flexibly supported structure is used. The flow is modelled with the system of Navier-Stokes equations written in Arbitrary Lagrangian-Eulerian form and coupled with system of ordinary differential equations describing the airfoil vibrations with two degrees of freedom. The Navier-Stokes equations are spatially discretized by the fully stabilized finite element method. The numerical results are shown.

1. Introduction

The gust-response analysis is important in the aircraft wing design, typically the wing have to withstand a gust of certain intensity and profile. As the aeroelastic effects can have significant influence on the gust loads, the aeroelastic analysis of gust response is important, cf. [1]. Modern methods for dynamic gust analysis typically rely on panel-method aerodynamics, where the frequency domain formulations are being used. In this paper the dynamic gust-response analysis is performed with the aid of the developed finite element code, and particularly the gust response of a flexibly supported very light airfoil was numerically analyzed. The mathematical model consists of fluid flow described by the two-dimensional Navier-Stokes equations and the continuity equation coupled with the equations describing the airfoil motion. The incompressible flow is approximated by the finite element method (FEM). The couple of finite element velocity/pressure spaces satisfies the Babuška-Breezi condition, see e.g. [6]. The dominating convection is stabilized by the residual based stabilization, cf. [5]. The numerical solution is sought on adaptively refined meshes, cf. [4]. The motion of the computational domain is treated by the Arbitrary Lagrangian-Eulerian (ALE) method, cf. ([8, 7]).

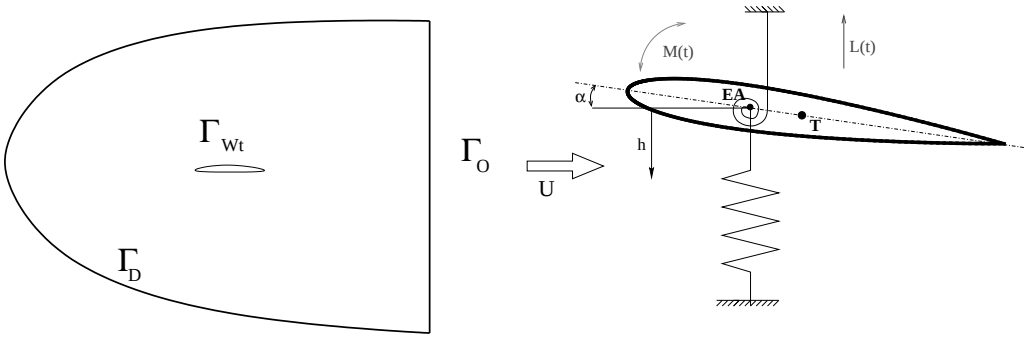

Figure 1: A sketch of the computational domain and its boundary (left). The elastic support of the airfoil on translational and rotational springs (right).

2. Mathematical model

Fluid flow. The flow in the two-dimensional computational domain Ω_t is described by the incompressible Navier-Stokes equations written in ALE form

$$\frac{D^{\mathcal{A}}\mathbf{u}}{Dt} + (\mathbf{u} - \mathbf{w}_D) \cdot \nabla \mathbf{u} + \nabla p - \nu \triangle \mathbf{u} = 0 \text{ in } \Omega_t, \qquad (1)$$
$$\nabla \cdot \mathbf{u} = 0 \text{ in } \Omega_t,$$

where $\frac{D^{\mathcal{A}}}{Dt}$ denotes the ALE derivative, $\mathbf{w}_D$ denotes the ALE domain velocity, $\mathbf{u} = (u_1, u_2)^T$ is the velocity vector, p is the kinematic pressure, and ν is the kinematic viscosity. The symbol $\mathcal{A}_t$ denotes a regular one-to-one Arbitrary Lagrangian-Eulerian (ALE) mapping of the reference configuration Ω_0 onto the current configuration Ω_t for any time instant $t \in I$. The boundary $\partial\Omega_t$ consists of mutually disjoint parts shown in Fig. 1, where Γ_D is the inlet part, Γ_O is the outlet boundary, and Γ_{Wt} is the moving surface of the airfoil, $\partial\Omega_t = \Gamma_D \cup \Gamma_O \cup \Gamma_{Wt}$. The system of equations (1) is completed with boundary conditions

$$\begin{aligned} &\text{a)} \quad \mathbf{u}(x,t) = \mathbf{u}_D + \mathbf{V}_g(t) \qquad \text{for } x \in \Gamma_D, \quad t \in I, \\ &\text{b)} \quad \mathbf{u}(x,t) = \mathbf{w}_D(x,t) \qquad \text{for } x \in \Gamma_{Wt}, \quad t \in I, \\ &\text{c)} \quad -\nu \tfrac{\partial \mathbf{u}}{\partial \mathbf{n}} + (p - p_{ref})\mathbf{n} = 0 \qquad \text{on } \Gamma_O, \end{aligned} \qquad (2)$$

where $\mathbf{u}_D = (U_\infty, 0)$ is the far field velocity, $\mathbf{V}_g(t)$ is the vertical gust velocity, p_{ref} is a reference mean value of pressure at the outlet part of boundary, and by an initial condition

$$\mathbf{u}(x,0) = \mathbf{u}_0(x), \qquad x \in \Omega_0. \qquad (3)$$

Structural model. The fluid flow is coupled with the motion of a flexibly supported airfoil, which can be vertically displaced and rotated. Fig. 1 shows the elastic support of the airfoil on translational and rotational springs. The pressure and viscous forces acting on the vibrating airfoil immersed in flow result in the lift force $L(t)$

and the torsional moment $M(t)$. The governing equations are written in the form (see [10])

$$\begin{aligned} m\ddot{h} + S_\alpha\,\ddot{\alpha} + k_{hh}h &= -L(t), \\ S_\alpha\ddot{h} + I_\alpha\ddot{\alpha} + k_{\alpha\alpha}\alpha &= M(t), \end{aligned} \tag{4}$$

where k_{hh} and $k_{\alpha\alpha}$ are the bending stiffness and torsional stiffness, respectively, m is the mass of the airfoil, S_α is the static moment around the elastic axis EA and I_α is the inertia moment around EA.

Coupling conditions. The aerodynamic lift force L acting in the vertical direction and the torsional moment M are defined by

$$L = -\,l\int_{\Gamma_{Wt}}\sum_{j=1}^{2}\tau_{2j}n_j dS, \qquad M = -\,l\int_{\Gamma_{Wt}}\sum_{i,j=1}^{2}\tau_{ij}n_j r_i^{\mathrm{ort}} dS, \tag{5}$$

where l is the depth of the considered airfoil section, and τ_{ij} are the components of the stress tensor defined by

$$\begin{aligned} \tau_{ij} &= \rho\left[-p\delta_{ij} + \nu\left(\frac{\partial u_i}{\partial x_j} + \frac{\partial u_j}{\partial x_i}\right)\right], \\ r_1^{\mathrm{ort}} &= -(x_2 - x_{\mathrm{EA2}}),\ r_2^{\mathrm{ort}} = x_1 - x_{\mathrm{EA1}}. \end{aligned} \tag{6}$$

In Eq. (6) by δ_{ij} the Kronecker symbol is denoted, $\mathbf{n} = (n_1, n_2)$ is the unit outer normal vector to $\partial\Omega_t$ on Γ_{Wt} (pointing into the airfoil) and $x_{\mathrm{EA}} = (x_{\mathrm{EA1}}, x_{\mathrm{EA2}})$ is the position of the elastic axis. Relations (5) and (6) define the coupling of the fluid model with the structural model.

3. Finite element approximation

The straightforward application of FEM procedures is often not possible for the incompressible Navier-Stokes equations particularly due to the advection-diffusion character of the equations with the dominating advection, for which a case the Galerkin FEM leads to unphysical solutions if the grid is not fine enough in regions of strong gradients. In order to obtain physically admissible correct solutions it is necessary to apply suitable mesh refinement (e.g. anisotropically refined mesh, cf. [4]) combined with a stabilization technique, cf. [2, 9]. In this work, the FEM is stabilized with the aid of streamline upwind/pressure stabilizing Petrov-Galerkin (SUPG/PSPG) method (so called *fully stabilized scheme*, cf. [5]) modified for the application on moving domains (cf. [10]). In order to discretize the problem (1), we define the equidistant division of the time interval $[0, T]$ with the time step Δt, denote $t_n = n\Delta t$, and approximate the time derivative by second order backward difference formula:

$$\frac{D^{\mathcal{A}}\mathbf{u}}{Dt}(x,t) \approx \frac{3\mathbf{u}^{n+1} - 4\widehat{\mathbf{u}^n} + \widehat{\mathbf{u}^{n-1}}}{2\Delta t},$$

where $\mathbf{u}^{n+1}$ is the approximation of the flow velocity at time t^{n+1} defined on the computational domain Ω^{n+1}, and $\widehat{\mathbf{u}^k}$ is the transformation of the flow velocity at time t^k defined on Ω^k transformed onto Ω^{n+1}. Further, equation (1) is formulated weakly and the solution is sought on the couple of finite element spaces $W_\Delta \subset \mathbf{H}^1(\Omega^{n+1})$ and $Q_\Delta \subset L^2(\Omega^{n+1})$ for approximation of velocity components and pressure, respectively. Further, by $X_\Delta \subset W_\Delta$ the subspace of the test functions is denoted. Let us mention that the finite element spaces should satisfy the *Babuška–Brezzi (BB) condition* (see e.g. [6]). In practical computations we assume that the domain $\Omega = \Omega^{n+1}$ is a polygonal approximation of the region occupied by the fluid at time t^{n+1} and the finite element spaces are defined over a triangulation $\mathcal{T}_\Delta$ of the domain Ω_t as piecewise polynomial functions. In our computations, the well-known Taylor-Hood P_2/P_1 conforming finite element spaces are used for the velocity/pressure approximation.

The *stabilized discrete problem* at a time instant $t = t^{n+1}$ reads: Find $U = (\mathbf{u}, p) \in W_\Delta \times Q_\Delta$, $p := p^{n+1}$, $\mathbf{u} := \mathbf{u}^{n+1}$, such that $\mathbf{u}$ satisfies approximately the Dirichlet boundary conditions (2 a-b) and

$$a(U; U, V) + \mathcal{L}(U; U, V) + \mathcal{P}(U, V) = f(V) + \mathcal{F}(U; V) \tag{7}$$

holds for all $V = (\mathbf{z}, q) \in X_\Delta \times Q_\Delta$. Here, the Galerkin terms are defined for any $U = (\mathbf{u}, p)$, $V = (\mathbf{z}, q)$, $U^* = (\mathbf{u}^*, p^*)$ by

$$\begin{aligned} a(U^*; U, V) &= \frac{3}{2\Delta t}(\mathbf{u}, \mathbf{z})_\Omega + \frac{1}{Re}(\nabla \mathbf{u}, \nabla \mathbf{z})_\Omega + (\overline{\mathbf{w}} \cdot \nabla \mathbf{u}, \mathbf{z})_\Omega - (p, \nabla \cdot \mathbf{z})_\Omega + (\nabla \cdot \mathbf{u}, q)_\Omega, \\ f(\mathbf{u}, \mathbf{z}) &= \frac{1}{2\Delta t}(4\hat{\mathbf{u}}^n - \hat{\mathbf{u}}^{n-1}, \mathbf{z})_\Omega, \end{aligned}$$

where $\overline{\mathbf{w}} = \mathbf{u}^* - \mathbf{w}_D^{n+1}$, and the scalar product in $L^2(\Omega)$ is denoted by $(\cdot, \cdot)_\Omega$. Further, the SUPG/PSPG stabilization terms are used in order to obtain stable solution also for large values of Reynolds numbers,

$$\begin{aligned} \mathcal{L}(U^*; U, V) &= \sum_{K \in \mathcal{T}_\Delta} \delta_K \left(\frac{3\mathbf{u}}{2\tau} - \frac{1}{Re}\triangle \mathbf{u} + (\overline{\mathbf{w}} \cdot \nabla)\mathbf{u} + \nabla p, (\overline{\mathbf{w}} \cdot \nabla)\mathbf{v} + \nabla q \right)_K, \\ \mathcal{F}(U^*; V) &= \sum_{K \in \mathcal{T}_\Delta} \delta_K \left(\frac{4\hat{\mathbf{u}}^n - \hat{\mathbf{u}}^{n-1}}{2\tau}, (\overline{\mathbf{w}} \cdot \nabla)\mathbf{v} + \nabla q \right)_K, \end{aligned}$$

where $\overline{\mathbf{w}} = \mathbf{v}^* - \mathbf{w}^{n+1}$, and $(\cdot, \cdot)_K$ denotes the scalar product in $L^2(K)$. The term $\mathcal{P}(U, V)$ is the additional grad-div stabilization defined by

$$\mathcal{P}(U, V) = \sum_{K \in \mathcal{T}_\Delta} \tau_K (\nabla \cdot \mathbf{u}, \nabla \cdot \mathbf{z})_K.$$

Here, the choice of the parameters $\delta_K \approx h_K^2$ and $\tau_K \approx 1$ is carried out according to [5] or [9] on the basis of the local element length h_K.

Furthermore, the nonlinear stabilized weak formulation of Navier-Stokes system (7) is solved with the aid of Oseen linearization. The arising large system of linear equations is solved by a direct solver as UMFPACK (cf. [3]).

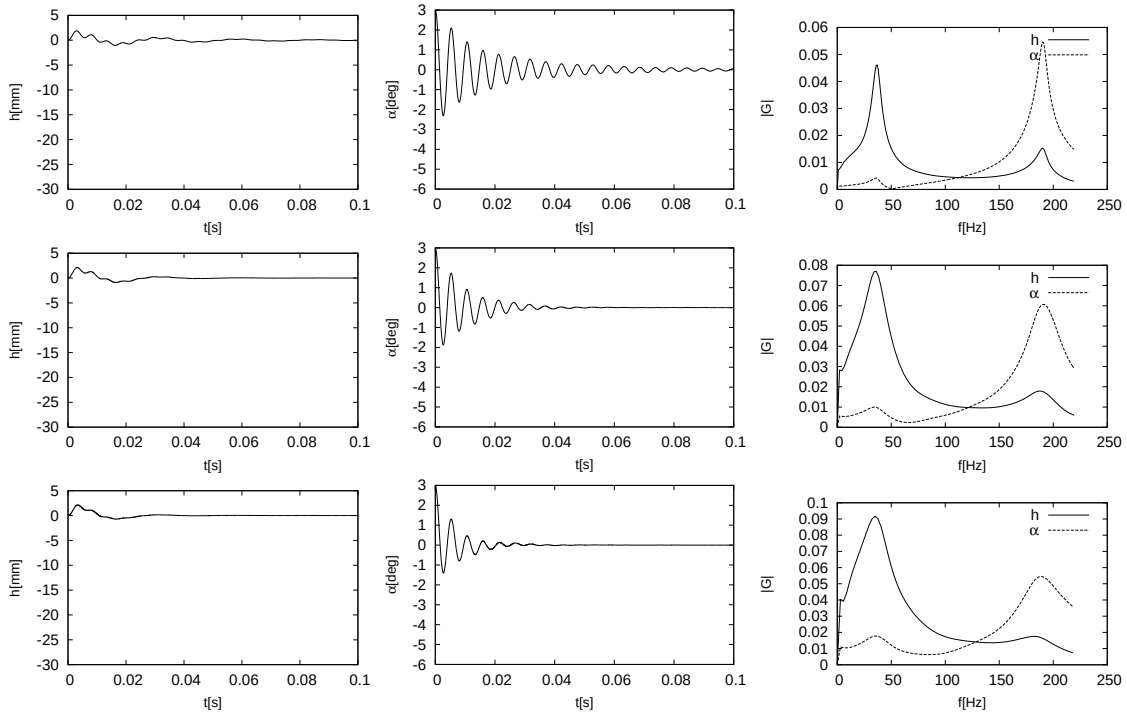

Figure 2: Aeroelastic response and its spectra for the far field velocity $U_\infty = 5\,\mathrm{m/s}$ (top), $U_\infty = 10\,\mathrm{m/s}$ (middle) and $U_\infty = 15\,\mathrm{m/s}$ (bottom).

The equations describing the motion of the flexibly supported airfoil are discretized in time by second order backward difference formula and the coupled fluid-structure model is solved using the partitioned strongly coupled algorithm. This means that per every time step the fluid flow and the structure motion are approximated repeatedly in order to converge to a solution which satisfies all interface conditions. In order to overcome the instability due to the coupling procedure, an underrelaxation is applied for the structural part of the problem.

4. Numerical results

The presented numerical method is applied for approximation of aeroelastic behaviour of a typical section, which is an idealized representation of a wing.

The structural parameters were chosen according to [1]. The aircraft wing structural arrangement is uniformly made of balsa wood (density $\rho = 150\,\mathrm{kg/m^3}$, Young modulus $E = 1.3\times10^9\,\mathrm{Pa}$, shear modulus $G = 6.2\times10^8\,\mathrm{Pa}$). The airfoil shape is given by the Karman-Trefftz conformal transformation, for details see [1]. The mass and inertial properties of the considered airfoil were $m = 2\times10^{-4}\,\mathrm{kg}$ and $I = 10^{-7}\,\mathrm{kg\ m^2}$. Thus $I_\alpha = 1.2\times10^{-7}\,\mathrm{kg\ m^2}$, $S_\alpha = 2\times10^{-6}\,\mathrm{kg\ m}$. The stiffness coefficients of the springs were $k_h = 25.4\,\mathrm{N/m}$, $k_\alpha = 0.272\,\mathrm{N\,m/rad}$. The airfoil chord was $c = 0.1\,\mathrm{m}$ and the depth of the section was $l = 0.03\,\mathrm{m}$. The air density was $\rho = 1.225\,\mathrm{kg\,m^{-3}}$ and the air kinematic viscosity was $\nu = 1.453\times10^{-5}\,\mathrm{m^2/s}$.

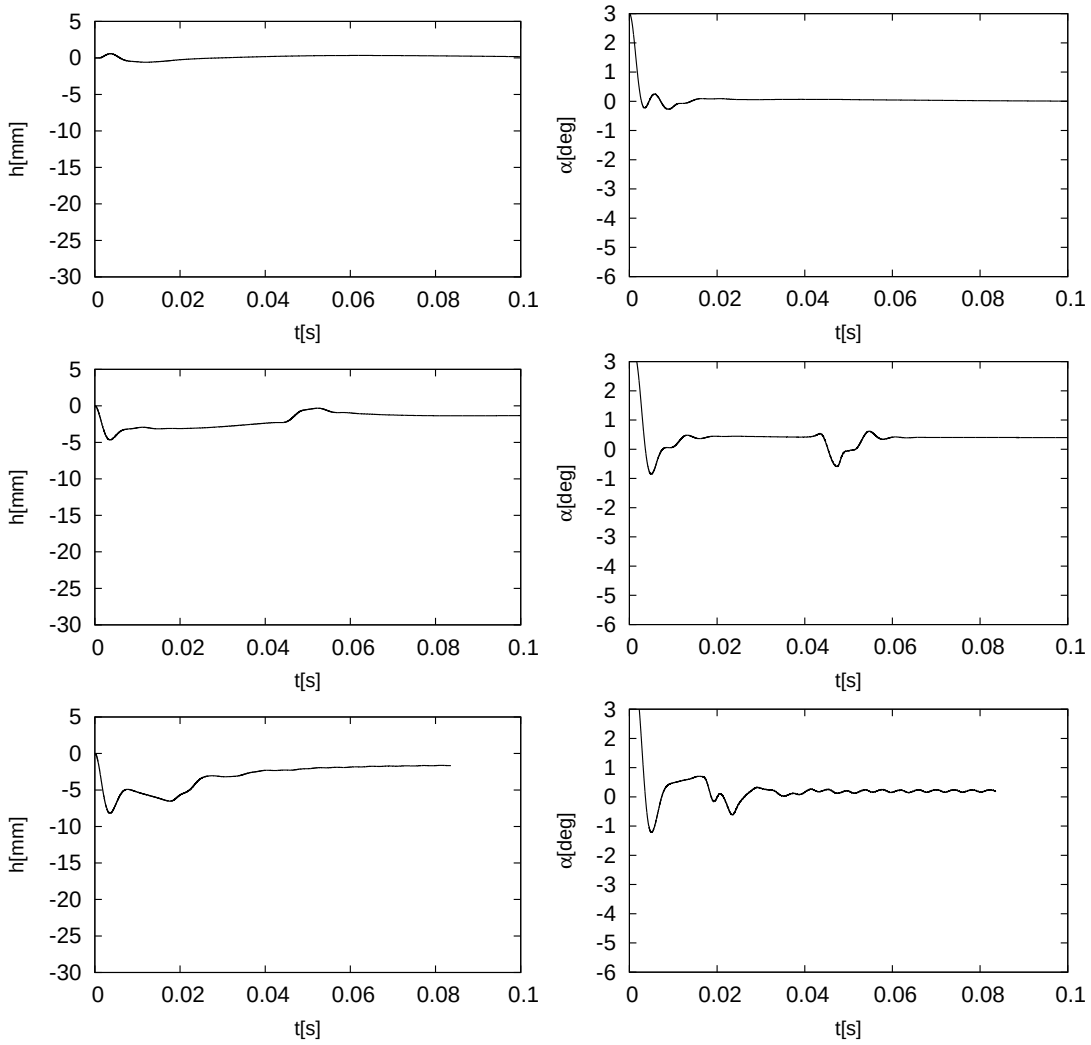

Figure 3: Aeroelastic response for the far field velocity $U_\infty = 30\,\mathrm{m/s}$ (top), $U_\infty = 50\,\mathrm{m/s}$ (middle) and $U_\infty = 60\,\mathrm{m/s}$ (bottom).

A vertical wind gust acts as the aerodynamic perturbation to the static equilibrium of the aeroelastic system and is introduced as a variation of the free-stream velocity prescribed on the inlet part of the boundary. A sinusoidal vertical gust of one-second duration is considered. The reference free stream velocity was chosen $U_\infty = 15\,\mathrm{m/s}$ and the gust intensity $V_G = 1.5\,\mathrm{m/s}$ for the light gust and $V_G = 5\,\mathrm{m/s}$ for the heavy gust case was considered.

The aeroelastic response of the considered airfoil computed for constant far field velocities and the initial conditions $\alpha(0) = 3°$, $h(0) = 0\,\mathrm{m}$, $\dot{h}(0) = 0\,\mathrm{m/s}$, $\dot{\alpha}(0) = 0°\mathrm{s}^{-1}$ are shown in Figs. 2 and 3. The spectra of the numerically simulated signals show the lower resonance frequency at about 36 Hz for predominantly vertical vibrations and at about 191 Hz for rotation of the airfoil. The damping of the system increases with higher flow velocities. The system is damped by aerodynamic forces and is stable for all the considered values of far field velocities up to $U_\infty = 60\,\mathrm{m/s}$.

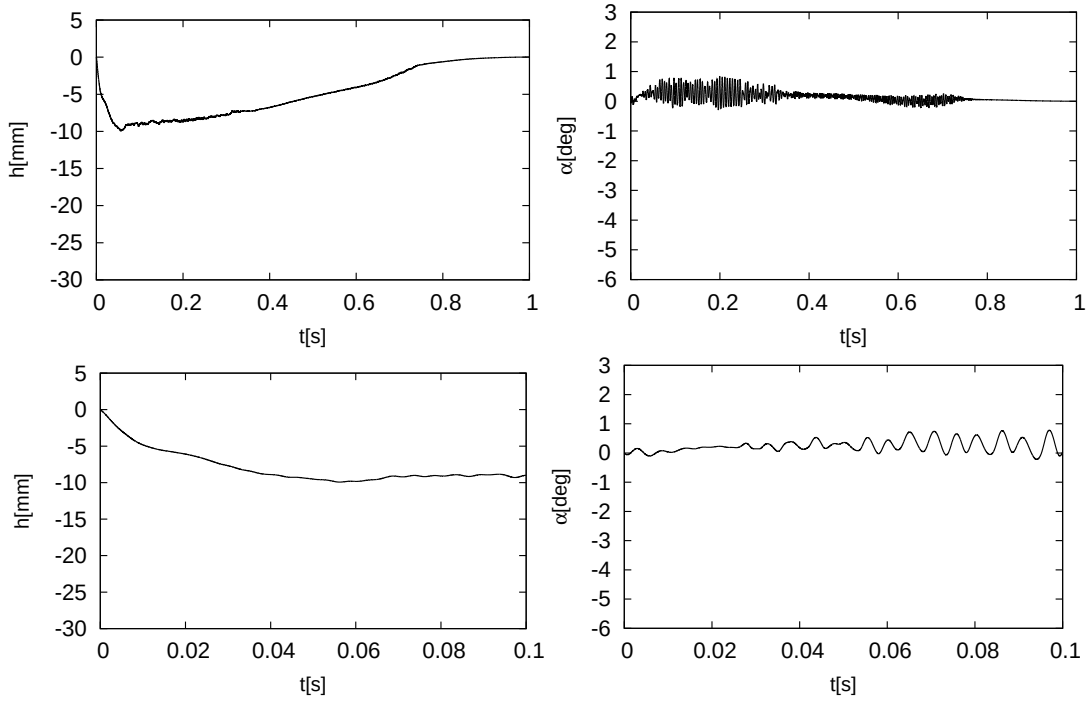

Figure 4: The numerical results for light gust. The aeroelastic response of the typical airfoil section for far field velocity $U_\infty = 15\,\mathrm{m/s}$ and gust velocity $V_G = 1.5\,\mathrm{m/s}$ (top). The detail of the response during the first 0.1 s (bottom).

The gust aeroelastic responses computed for the cases of either a light ($V_G = 1.5\,\mathrm{m/s}$) or a heavy gust ($V_G = 5\,\mathrm{m/s}$) are shown in Figs. 4 and 5. For the case shown in Fig. 5 the flow velocity patterns are shown in Fig. 6, where a very strong vorticity above the vibrating profile was developed after the airfoil loading by the heavy gust.

5. Discussion and conclusion

The gust response of a typical airfoil section has been investigated with the aid of a developed numerical scheme. The numerical method was described and the numerical results of a benchmark problem were presented.

The aeroelastic gust responses exhibit stronger oscillations than it was found by Berci et al. [1]. The maximum of the airfoil rotation amplitude for a light gust resulting from our computation ($\alpha \approx 0.8°$) was found nearly three time higher than the maximum rotation ($\alpha \approx 0.27°$) computed in [1], however, a maximum of a mean value for rotation ($\alpha \approx 0.3°$) is in a good agreement with the results by Berci et al. Similarly, the maximum value of the computed vertical displacement $h \approx 10\,\mathrm{mm}$ approximately correspond to a maximum $h \approx 8\,\mathrm{mm}$ found in [1]. A dominant oscillation frequency corresponds to the airfoil rotation.

Similar conclusions result from the computation of the airfoil response to a heavy gust. The maximum values for the horizontal displacement of about $h \approx 30\,\mathrm{mm}$

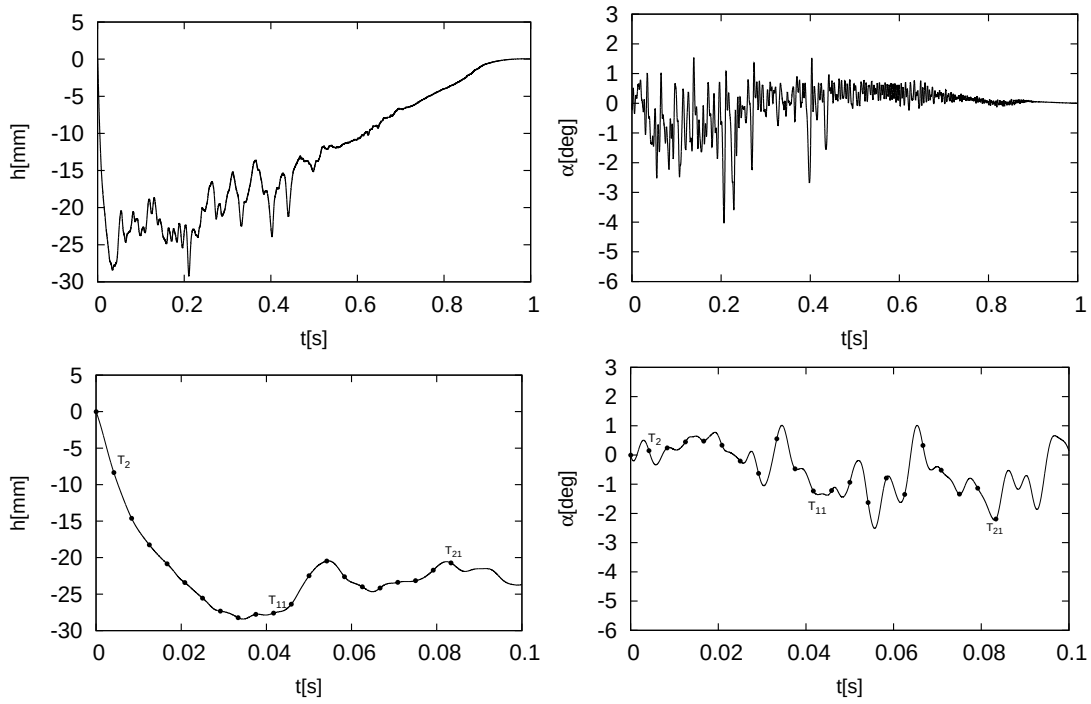

Figure 5: The numerical results for heavy gust. The aeroelastic response of the typical airfoil section for far field velocity $U_\infty = 15\,\mathrm{m/s}$ and gust velocity $V_G = 5\,\mathrm{m/s}$ (top). The detail of the response during the first 0.1 s (bottom).

computed by us correspond well to the maximum value $h \approx 27\,\mathrm{mm}$ obtained in [1]. The maxima of mean values computed for rotation ($\alpha \approx 1°$) are in a good agreement in both studies, however, the maximum value for rotation computed in our case ($\alpha \approx 4°$) is evidently higher than the maximum $\alpha \approx 2.5°$ found in [1].

The reason for the found differences between the two approaches of the numerical simulation can be mainly in the flow model. Berci et al. [1] considered Reynolds Average Navier Stokes equations (RANS) including a turbulence model for the flow and we considered the laminar flow, when the flow separation on the airfoil surface is becoming earlier and creation of the vortices is more frequent than in the case of turbulent boundary layer.

Acknowledgements

This work was supported by grant No. P101/11/0207 of the Czech Science Foundation.

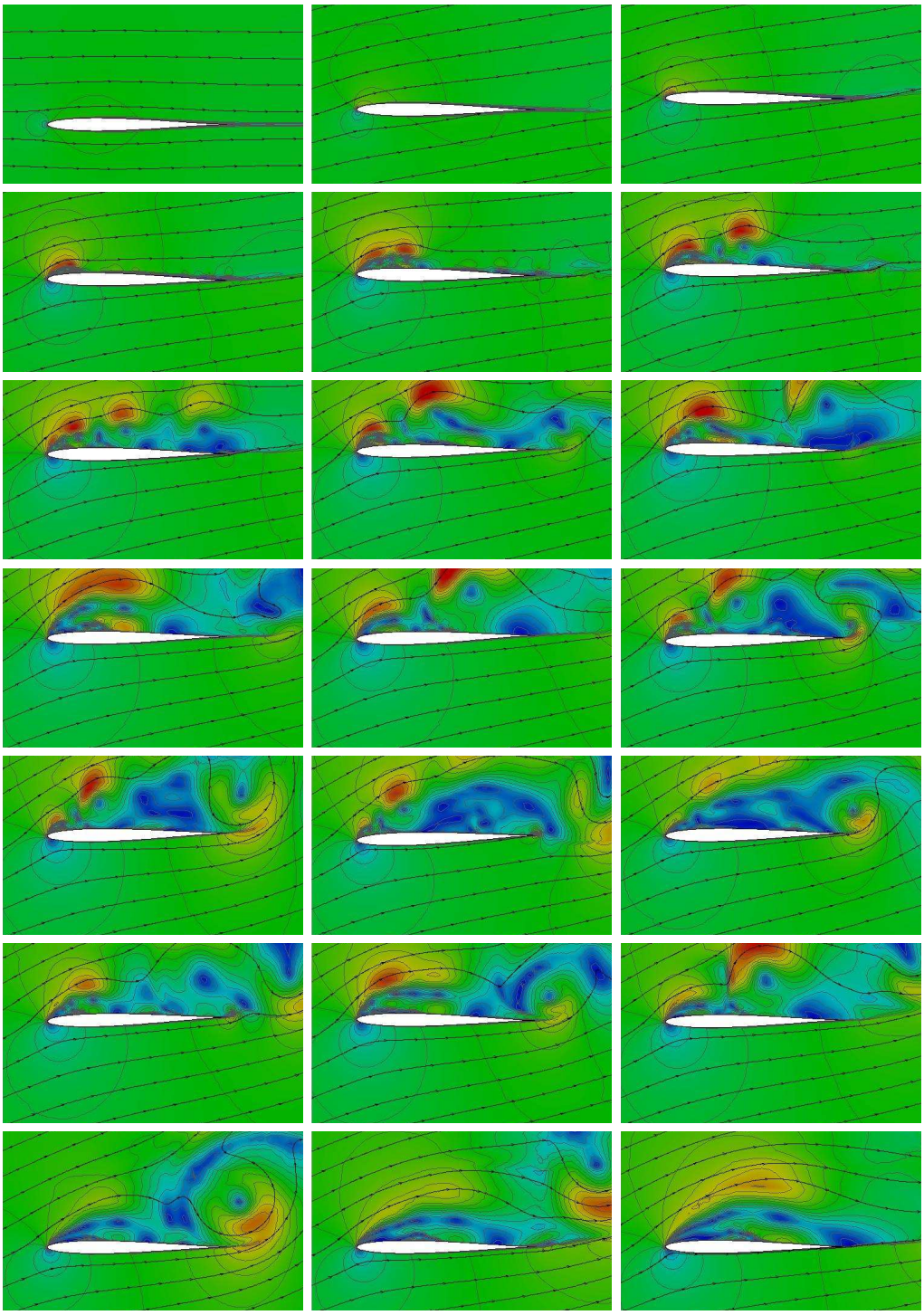

Figure 6: The flow pattern at the equidistant time instants $T_k = k\Delta T$ marked in Fig. 5, $\Delta T = 2 \times 10^{-4}$ s.

References

[1] Berci, M., Mascetti, S., Incognito, A., Gaskell, P. H., and Toropov, V. V.: Gust response of a typical section via CFD and analytical solutions. In: J. C. F. Pereira and A. Sequeira (Eds.), *ECCOMAS CFD 2010, V. European Conference on Computational Fluid Dynamics*, 2010.

[2] Codina, R.: Stabilization of incompressibility and convection through orthogonal sub-scales in finite element methods. Comput. Method Appl. Mech. Engrg. **190** (2000), 1579–1599.

[3] Davis, T. A. and Duff, I. S.: A combined unifrontal/multifrontal method for unsymmetric sparse matrices. ACM Trans. Math. Software **25** (1999), 1–19.

[4] Dolejší, V.: Anisotropic mesh adaptation technique for viscous flow simulation. East-West J. Numer. Math. **9** (2001), 1–24.

[5] Gelhard, T., Lube, G., Olshanskii, M. A., and Starcke, J. H.: Stabilized finite element schemes with LBB-stable elements for incompressible flows. J. Comput. Appl. Math. **177** (2005), 243–267.

[6] Girault, V. and Raviart, P. A.: *Finite element methods for the Navier-Stokes equations*. Springer, Berlin, 1986.

[7] Le Tallec, P. and Mouro, J.: Fluid structure interaction with large structural displacements. Comput. Method Appl. Mech. Engrg. **190** (2001), 3039–3067.

[8] Nomura, T. and Hughes, T. J. R.: An arbitrary Lagrangian-Eulerian finite element method for interaction of fluid and a rigid body. Comput. Method Appl. Mech. Engrg. **95** (1992), 115–138.

[9] Sváček, P. and Feistauer, M.: Application of a stabilized FEM to problems of aeroelasticity. In: *Numerical Mathematics and Advanced Application*, pp. 796–805. Springer, Berlin, 2004.

[10] Sváček, P., Feistauer, M., and Horáček, J.: Numerical simulation of flow induced airfoil vibrations with large amplitudes. J. Fluids and Structures **23** (2007), 391–411.